Theory of unconventional magnetism in a Cu-based kagome metal

Anja Wenger,[1] Armando Consiglio,[2] Hendrik Hohmann,[1] Matteo Dürrnagel,[1,3,*] Fabian O. von Rohr,[4] Harley D. Scammell,[5] Julian Ingham,[6] Domenico Di Sante,[2,7] and Ronny Thomale[1,†]

[1]*Institut für Theoretische Physik und Astrophysik and Würzburg-Dresden Cluster of Excellence ct.qmat, Universität Würzburg, 97074 Würzburg, Germany*

[2]*Istituto Officina dei Materiali, Consiglio Nazionale delle Ricerche, Trieste I-34149, Italy*

[3]*Institute for Theoretical Physics, ETH Zürich, 8093 Zürich, Switzerland*

[4]*Department of Quantum Matter Physics, University of Geneva, CH-1211 Geneva, Switzerland*

[5]*School of Mathematical and Physical Sciences, University of Technology Sydney, Ultimo NSW 2007, Australia*

[6]*Department of Physics, Columbia University, New York, New York 10027, USA*

[7]*Department of Physics and Astronomy, University of Bologna, 40127 Bologna, Italy*

(Received 7 November 2024; revised 16 September 2025; accepted 21 October 2025; published 8 December 2025)

Kagome metals have established a new arena for correlated electron physics. To date, the predominant experimental evidence centers around unconventional charge order, nematicity, and superconductivity, while magnetic fluctuations due to electronic interactions, i.e., beyond local atomic magnetism, have largely been elusive. We find the challenge of locating the appropriate parameter regime for such exotic order to center around two aspects. First, the correlations implied by low-energy orbitals have to be sufficiently large to yield a dominance of magnetic fluctuations and sufficiently weak to retain an itinerant parent state. Second, the kinematic kagome profile at the Fermi level demands an efficient mitigation of sublattice interference causing the suppression of magnetic fluctuations descending from electronic on-site repulsion. We elucidate our methodology by analyzing the potential copper-based kagome compound $CsCu_3Cl_5$: From *ab initio* design and many-body analysis, we develop a model framework of realistic Cu-based kagome materials, the simulations of which reveal unconventional magnetic order in a kagome metal.

DOI: 10.1103/fszl-7g57

I. INTRODUCTION

The kagome lattice, characterized by its repeating pattern of corner-sharing triangles, forms a hexagonal network with three distinct sublattices. This unique geometry gives rise to exotic quantum phenomena, rendering it an exclusive host for correlated and topologically nontrivial electronic states. Depending on the balance between electronic interactions and kinetic energy, electronic models on the kagome lattice can yield myriad distinct physical phases. Kagome compounds with a metallic parent state generically feature intricate nonmagnetic phases such as exotic charge orders, nematicity, and superconductivity [1–6]. Most extensively discussed is the AV_3Sb_5 family ($A = $ K,Rb,Cs), in which the lack of magnetic order is best explained by both electron-phonon coupling effects [7,8] and the suppression of on-site Coulomb repulsion due to the sublattice interference (SI) mechanism, preventing local scattering channels between the van Hove singularities (vHS) [9–11]. This leads to a rich zoology of unconventional phases like charge bond (CBO) and loop current orders (LCO), which are largely not found in alternative correlated electron material domains such as cuprate or iron-pnictide compounds [12–14]. Due to the predominance of nonmagnetic phases, however, magnetic instabilities that might be unique to kagome kinematics have remained largely unexplored at the microscopic and even at the phenomenological level.

The emergence of magnetic instabilities requires a sufficient degree of electronic correlations. For strong electron-electron interactions, the electrons become Mott-localized on atomic sites, where unpaired spins create magnetic moments. The inherent geometric frustration of the kagome lattice leads to unconventional magnetic orders such as spin liquid phases. The most prominent example is Herbertsmithite [$ZnCu_3(OH)_6Cl_2$] [15,16], which lies deep in the Mott-insulating regime, rendering the unique features of the kagome band structure like vHS and Fermi surface nesting—which drive unconventional charge order in the itinerant case—irrelevant.

In this article, we aim to fuse the intricacies of electronic kagome kinematics with the potential emergence of magnetic order. We identify intermediately correlated kagome compounds close to the mixed *m*-type van Hove filling as a suitable system to stabilize exotic magnetic orders that inherit substantial nonlocal spin expectation values from the partial sublattice polarization of the Fermi surface. From detailed electronic structure calculations, we find that Cu-based 135-kagome compounds, i.e., $CsCu_3Cl_5$, provide a playground for exploring the potential realization of unconventional magnetic order in a realistic material setting. The low-energy physics of $CsCu_3Cl_5$ is well described by an isolated set of three bands with an *m*-type vHS close to the Fermi level, and it exhibits correlations intermediate between Herbertsmithite

*Contact author: matteo.duerrnagel@uni-wuerzburg.de
†Contact author: ronny.thomale@uni-wuerzburg.de

and the weakly correlated AV_3Sb_5 compounds. While Cu-O complexes are likely to be located in the Mott-localized regime, we propose that Cu-Cl complexes strike the aspired compromise between maximum interaction strength while preserving metallicity. Our analysis of the magnetic phase diagram unveils $CsCu_3Cl_5$ as a realistic material platform to host correlation-driven spin-bond order and highlights the broader implications of Fermi surface topology for exotic magnetic phases in kagome systems.

II. MODEL REALIZATION

Our theoretical platform $CsCu_3Cl_5$ is isostructural with other members of the 135 family, such as AV_3Sb_5, and crystallizes in the hexagonal space group $P6/mmm$ (No. 191). It features an in-plane kagome network of copper atoms, coordinated octahedrally by chlorine atoms, forming layered Cu_3Cl_5 sheets that are separated along the $\hat{c}$-axis by a triangular net of cesium ions. $CsCu_3Cl_5$ exhibits a mixed valence state, where copper ions are present in both Cu(I) and Cu(II) oxidation states, with an average oxidation state of $+1.33$.

While Cu generally prefers the +II oxidation state, as observed in the chemically related phases Cs_2CuCl_4 [17] and $CsCuCl_3$ [18], the presence of Cu(I) in compounds such as $Cs_3Cu_2Cl_5$ [19] supports the feasibility of this mixed valence state. A notable point is the possibility of a mixed charge on a crystallographic site. Whether this is statistically distributed in the structural model or whether some form of ordering is present remains an open question. The ionic radii of Cu(I) and Cu(II) in octahedral coordination do not differ significantly, making this mixed occupation proposed here certainly plausible [20]. Due to its full d^{10} electron configuration, Cu(I) lacks the electronic degeneracy needed for Jahn-Teller distortions, making it less prone to such distortions compared to Cu(II). In contrast, Cu(II), with its d^9 electron configuration, is a well-known Jahn-Teller ion and typically undergoes bond elongations or compressions in its octahedral coordination environment to lower its energy [21]. It is also worth noting that Cu(I), at least in chloride environments, does not always form regular coordination polyhedra. This irregularity might stem from the nature of Cs-Cl compounds, where the large size of Cs ions can sometimes influence the coordination environments of surrounding atoms, though such effects are less likely in layered structures like those in $CsCu_3Cl_5$. A thorough analysis of the compound's stability reveals the pristine configuration as a metastable state. However, the analysis of single-particle and derived many-body effects in the energetically favored twisted configuration matches qualitatively the results for the pristine case. To maintain generality, we explicate in the following a study of the pristine structure and refer the interested reader to the Supplemental Material (SM) [22] for the analogous treatment of the twisted configuration.

Despite being isostructural to other members of the 135 family like AV_3Sb_5, the calculated electronic band structure, shown in Fig. 1(c), reveals striking differences from previous reports on known kagome compounds. The characteristic kagome band manifold—including a flat band, a Dirac point located at the K-point, and two vHSs at each of the three inequivalent M-points—appears well separated from other bands at low energies. The orbital projection of the band

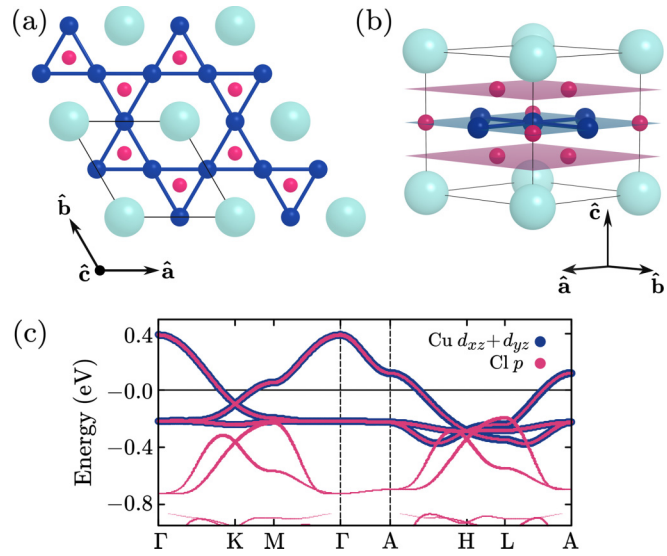

FIG. 1. Crystal structure of pristine $CsCu_3Cl_5$. (a) Top view showing the Cu kagome lattice highlighted by blue bonds. Turquoise, blue, and pink spheres represent Cs, Cu, and Cl atoms. The unit cell is delimited by black lines. (b) Side view of the unit cell. The blue plane contains the Cu kagome lattice and additional Cl atoms, while the pink planes above and below contain a hexagonal lattice of Cl atoms. (c) Electronic band structure with projected orbital weights featuring distinct kagome bands and an m-type vHS close to E_F.

structure illustrates that the states at E_F emerge only from the hybridization of the out-of-plane Cu d_{xz} and d_{yz} orbitals with Cl p orbitals. This can be attributed to a collaborative effect: The enhanced valence of Cu (d^9) suggests a single kagome band manifold close to the Fermi level in analogy to ATi_3Bi_5 ($A = $ Cs, Rb) [23–25], where the d^1 configuration of Ti constitutes the analog of Cu. In $CsCu_3Cl_5$, however, the strong polar Cu-Cl bonding results in an enhanced crystal-field splitting, which separates partially filled valence bonds from fully filled bonding and empty antibonding states.

This is directly reflected in the real-space arrangement of chlorine atoms around each copper atom, forming a distorted octahedron, elongated by 0.21 Å towards the center of the hexagonal plaquette (see the SM). Within the octahedra, the spatial proximity of the Cu d-orbitals and Cl p-orbitals induces a pronounced splitting in the d-orbital energy levels. Both effects produce a uniquely isolated and undistorted kagome band structure close to the Fermi level. In addition, $CsCu_3Cl_5$ is distinct from related 135 compounds by its inverted band ordering, with the flat band at the bottom [Fig. 1(c)]. This sets an m-type vHS in the vicinity of the Fermi level, opposed to the widely studied p-type variant, with important consequences upon the inclusion of interaction effects.

III. ELECTRONIC CORRELATIONS ACROSS KAGOME COMPOUNDS

The members of the 135 family are generally considered weakly correlated, where phonons play a crucial role in charge ordering mechanism in collaboration or competition with electronic interactions [26,27].

To estimate interaction parameters from first principles, we perform constrained random phase approximation (cRPA) calculations [28–31] for pristine $CsCu_3Cl_5$ (see the SM [22] for details and results for the twisted configuration), using as the target space a set of Wannier functions derived from the Wannier model described later in this paper. The resulting screened on-site effective Coulomb interaction is $U = 3.6\,\text{eV}$ (bare on-site Coulomb interaction $U_{\text{bare}} = 14.7\,\text{eV}$). With the quite narrow bandwidth t, this yields a ratio $U/t \approx 4.7$, placing $CsCu_3Cl_5$ above the weakly correlated AV_3Sb_5 compounds with $U/t < 1$ [31] and well below the strongly correlated Herbertmithite in the region of $U_{\text{bare}}/t \approx 20$ [32]. The qualitative findings are consistent with a bond length analysis [33], which estimates the relative degree of correlation across various kagome compounds by the transition metal to ligand distance as explicated in the SM. This classification aligns well with the picture that a larger filling fraction of the $3d$ shell in copper compared to Ti (d^1) [24], V (d^3) [34], or Cr (d^4) [35] as the central block of the kagome network can enhance local correlations.

A notable exception to this rule is presented by $CsCr_3Sb_5$, which displays an admixture of charge and magnetically ordered phases at low temperatures [35,36]: Contrary to other members of the 135 family, this compound features a flat band in the vicinity of the Fermi level [37]. The large spectral weight close to the Fermi level significantly enhances magnetic fluctuations and drives the system to strong coupling irrespective of the U over bandwidth ratio [38–40]. Consequently, it is not only the bare interaction strength inside the correlated manifold that plays a crucial role in determining the degree of correlations in a material. Likewise, the available low-lying states for electronic scattering processes play a decisive role beyond crystal-field effects. In particular, pronounced Fermi surface nesting can drive the system to stronger coupling as canonically encountered close to vH filling. In kagome compounds, the nontrivial quantum geometry of the electronic eigenstates around the vHS points adds an additional layer of inference to the estimation of correlation strengths: In V-based 135 kagome compounds, the low-lying vHS is of pure p-type, i.e., each vHS point is exclusively supported by electronic states on one of the three kagome sublattice sites [10,11]. This reduces the effectiveness of local Coulomb interactions in driving Fermi surface instability via the celebrated sublattice interference (SI) mechanism [9,12] with two important corollaries for the AV_3Sb_5 family: First, the enhanced relevance of nonlocal Coulomb interactions leads to the absence of phases involving local particle-hole pairs at intermediate coupling [41,42]. Second, phonon coupling arising from a delocalized charge density across the sublattices gains significant importance, making it difficult to discern whether the observed instabilities are driven by phonons or electronic correlations [43,44].

IV. VAN HOVE SCATTERING AT M-TYPE FILLING

In $CsCu_3Cl_5$, the much less studied m-type vHS promotes a qualitatively different behavior. The sublattice occupation at the upper van Hove filling of $CsCu_3Cl_5$ is indicated in Fig. 2(d). At the three inequivalent van Hove points M_γ,

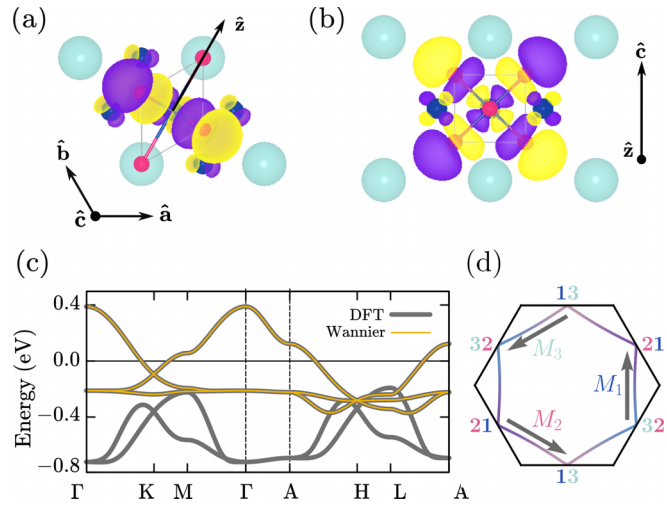

FIG. 2. Wannier orbital centered at the Cu site seen from (a) the top and (b) the side view of the pristine structure. The site-local reference axis $\hat{\mathbf{z}}$ is pointing towards the center of the hexagonal plaquettes. Purple/yellow orbital lobes indicate the phase of the MLWF. (c) Comparison of the DFT band dispersion (gray) with bands obtained from the Wannier three-orbital tight-binding model (yellow). (d) Fermi surface in the $k_z = 0$ plane for the noninteracting band structure at the upper vH filling and dominant nesting vectors. The colors indicate the eigenstate contributions on the three different sublattices. At the three M points, i.e., the vH points, the state is equally composed of two sublattices given by the sublattice labels.

the electronic states are equally distributed across two of the three sublattices with vanishing contribution on the third one. This configuration is known as a mixed m-type van Hove singularity [9]. Under scattering with $\mathbf{q} = \text{M}$, the electronic eigenstates at a vHS point transition to states comprised of a different combination of two sublattices. This ensures that one sublattice is occupied both before and after scattering and allows on-site interactions to mediate vHS nesting processes. While this weakens the effect of SI compared to the p-type case, on-site scattering is still partially restricted, as the local Hubbard interaction U acts only on one of the three sublattices at each inequivalent M-point. In the same way, the nearest-neighbor (NN) interaction V can mediate scattering between one defined pair of sublattices. Hence, scattering events with the nesting vector M_γ with $M_\alpha = M_\beta + M_\gamma$ between the vH points can be decomposed into a site local and nonlocal component

$$\langle u(M_\alpha)|\langle u(M_\alpha)|\Gamma_{o_1o_2o_3o_4}(M_\gamma)|u(M_\beta)\rangle|u(M_\beta)\rangle = \Gamma_{\gamma\gamma\gamma\gamma}(M_\gamma) + \Gamma_{\alpha\alpha\beta\beta}(M_\gamma). \quad (1)$$

Here, $u(M_\alpha)$ is the eigenstate of the noninteracting Hamiltonian at the vH point M_α and Γ the two-particle interaction. Thereby, both interaction scales, U and V, operate at similar scales due to the effect of the partial sublattice polarization of the vH points. This leads to a regime where both local and nonlocal interactions contribute significantly, and U and V are of comparable importance. Moreover, the m-type vHS corresponds to a more localized electronic structure in momentum space [9,12,13]. As a result, electrons couple less efficiently to

phonons, suppressing phonon-driven instabilities and making electronic correlations more effective.

The correlation strength within the low-energy manifold of $CsCu_3Cl_5$ is therefore anticipated to reside in a sweet spot between that of the weakly correlated CsV_3Sb_5, and the strongly correlated Herbertsmithite.

V. WANNIER MODEL

The isolated nature of the three characteristic kagome bands allows us to capture the electronic structure of $CsCu_3Cl_5$ around E_F with a single orbital per kagome site. To construct a tight-binding model with maximally localized Wannier functions (MLWFs), we begin with an initial approximation using a linear combination of d_{xz} and d_{yz} orbitals. After the spread minimization, three MLWFs are obtained, each centered on a distinct site of the kagome lattice and oriented within the central plane of the coordinating octahedra. These MLWFs share identical shapes, originating from a linear combination of the $d_{x^2-y^2}$ orbital (in the local reference frame of this site) and Cl p-orbitals. Details on the orientations of the local reference frames are provided in the SM. An example MLWF is illustrated in Figs. 2(a) and 2(b) with the orientation of the corresponding octahedron outlined in gray. $\hat{\mathbf{a}}$, $\hat{\mathbf{b}}$, $\hat{\mathbf{c}}$ span the (global) reference frame of the crystal, while $\hat{\mathbf{z}}$ aligns with the octahedron axis. The three MLWFs map onto each other under 60° rotation. These orbitals reflect the B_{2g} elementary band representation of $P6/mmm$, well separated from B_{3g} by the pronounced Jahn-Teller distortion described above [45].

By extracting bands from this three-orbital tight-binding model and comparing them with DFT band calculations in Fig. 2(c), we observe a perfect alignment of the bands, combined with a very small spread. This allows for a description using MLWF, making the three-orbital description a simple and well-suited model for many-body calculations. To study possible instabilities of $CsCu_3Cl_5$, we equip the noninteracting theory with two particle interactions. Following the discussion of the preceeding section and preceeding works on the kagome lattice [12,13,42], we choose bare interactions consisting of on-site U and NN repulsion V,

$$\hat{H}_I = U \sum_{\mathbf{i}} \hat{n}_{\mathbf{i}\uparrow}\hat{n}_{\mathbf{i}\downarrow} + V \sum_{\langle \mathbf{i},\mathbf{j}\rangle,\sigma\sigma'} \hat{n}_{\mathbf{j}\sigma}\hat{n}_{\mathbf{i}\sigma'}, \tag{2}$$

where $\hat{n}_{\mathbf{j}\sigma} = \hat{c}^\dagger_{\mathbf{j}\sigma}\hat{c}_{\mathbf{j}\sigma}$ is the fermionic number operator on site $\mathbf{j}$ with spin σ. As discussed above, the reduced SI at the m-type vHS—compared to the extensively investigated p-type scenario—allows local and long-range interactions to contribute on a more equal footing. Hence, V cannot be simply neglected, as done, e.g., in Ref. [46].

VI. MANY-BODY ANALYSIS OF MAGNETIC INSTABILITIES

The small number of bands crossing the Fermi level and the absence of local degrees of freedom in the Wannierized model make it well-suited for exploring the system's ordering tendencies using numerical many-body methods. We perform functional renormalization group (FRG) calculations, utilizing the truncated unity implementation provided by the divERGe code base [47]. The FRG provides a well-defined interpolation from the noninteracting model to a low-energy effective theory near the Fermi level by successively integrating out high-energy degrees of freedom [48,49]. During this RG flow, all quantum fluctuations involving states outside this restricted manifold are incorporated in the screening of the effective two-particle interaction. This is achieved within the FRG by a perturbative expansion of the possible scattering processes, which allows for an unbiased treatment of symmetry-breaking transitions in the superconducting, charge, and magnetic channel. This makes FRG a distinguished method for weak to intermediate coupling strengths, i.e., the interaction regime suitable for the exploration of itinerant magnetic orders. Further details on the FRG calculations can be found in the SM.

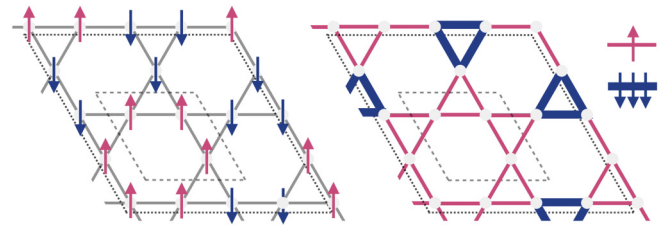

FIG. 3. Magnetic ordering vector of the Cu kagome network as obtained from combined FRG + GL analysis at m-type vH filling. The order parameter blends a collinear antiferromagnetic arrangement of local magnetic moments given in Eq. (3) (left) and NN spin bond terms of Eq. (4) (right) reminiscent of a tri-hexagonal pattern. Here, red/blue denote spin up/down on the indicated sites and bonds along the chosen quantization axis. While the relative strength of on-site ($\vec{\Delta}^{\mathrm{SDW}}$) and bond magnetization ($\vec{\Delta}^{\mathrm{SBO}}$) is dependent on the interaction parameter, their relative sign is fixed by the many-body analysis. To maintain vanishing net magnetization, the spin polarization on the ↓ bonds surpasses the value on the ↑ bonds by a factor of 3, as indicated by the line thickness.

Our FRG analysis reveals a $2 \times 2 \times 1$ magnetic order depicted in Fig. 3, which can be traced to a collaborative effect of two interaction length scales which operate at equal strength for an m-type vHS. The on-site U favors the formation of local spin polarization to avoid double occupancy on the sublattice site—this leads to long-range antiferromagnetic order at the Fermi surface nesting vector $\mathbf{M}_\gamma$ on the sublattice sites γ that do not suffer from SI. Meanwhile, NN V promotes the coupling of adjacent sites and generically favors bond orders over local particle-hole pairs, as known from the p-type vHS scenario [9]. This results in a magnetic state $\vec{\Delta}_\gamma = \vec{\Delta}^{\mathrm{SDW}}_\gamma + \vec{\Delta}^{\mathrm{SBO}}_\gamma$ that combines spin density wave order (SDW),

$$\vec{\Delta}^{\mathrm{SDW}}_\gamma \propto \sum_{\mathbf{i}} \cos(\mathbf{i}\cdot\mathbf{M}_\gamma)\langle \hat{c}^\dagger_{\mathbf{i}\gamma\sigma}\vec{\sigma}^{\sigma\sigma'}\hat{c}_{\mathbf{i}\gamma\sigma'}\rangle \tag{3}$$

with finite relative angular momentum components

$$\vec{\Delta}^{\mathrm{SBO}}_\gamma \propto \sum_{\langle \mathbf{i},\mathbf{j}\rangle} \cos(\mathbf{i}\cdot\mathbf{M}_\gamma)\Delta^{\mathbf{ij}\alpha\beta}_\gamma \langle \hat{c}^\dagger_{\mathbf{i}\alpha\sigma}\vec{\sigma}^{\sigma\sigma'}\hat{c}_{\mathbf{j}\beta\sigma'}\rangle, \tag{4}$$

that constitute a spin bond order phase (SBO). Here, $\langle \mathbf{i},\mathbf{j}\rangle$ is the sum over unit cell vecors $\mathbf{i},\mathbf{j}$ such that $\mathbf{i},\alpha$ and $\mathbf{j},\beta$ describe neighboring sites, and all doubly occurring indices

are summed over. The real-space representations of the SBO order parameter $\Delta_{\gamma}^{\mathbf{ij}\alpha\beta}$ are given in the SM.

At the M-point, the associated little group to the point group $P6/mmm$ is given by mmm, which is equivalent to the local symmetry group of the individual kagome sites on the $3f$ Wyckoff positions. Consequently, the SDW order parameter, which transforms trivially under all elements of mmm, has support only on sublattice γ. To mix with the U driven on-site magnetization, the SBO phase transforms within the A_g irreducible representation of mmm and thus represents an extended s-wave magnetization pattern. This is a crucial precondition for the magnetic state to lower its free energy via spin fluctuations of both local and nonlocal moments present in the m-type vH scenario. Contrarily, the p-type scenario does not allow for a local moment formation at the Fermi level due to SI [9]. While the p-type scenario opens up opportunities for bond-magnetization in nontrivial irreducible representations, it also limits the available free-energy gain, since the spin polarization exhibits a strong momentum dependence with additional nodes in the quasiparticle spectrum, which cannot contribute from the dominant on-site repulsion U.

A Ginzburg-Landau (GL) analysis (cf. the SM) shows that near the onset of magnetic order, the favored state is a collinear order in which SDW and SBO point along the same axis (Fig. 3), and modulate with a star-of-David pattern. The magnetic arrangement breaks Z_4 translation and spin rotation symmetries, and transforms within the three-dimensional F_2' irrep of the extended C_{6v}''' symmetry group of the enlarged 2×2 unit cell [50]. While retaining the original $P6/mmm$ symmetry, the superposition of the three different A_g states leads to a triple enhancement of the hexagonal bonds compared to the starlike bonds to ensure vanishing net magnetization. This marks the first instance of spontaneous magnetization in kagome metals driven by quantum fluctuations.

VII. INDUCED SPIN CURRENT ORDER

This change of paradigm—from the local moment-driven to itinerant magnetism—comes with the promise of more, yet unprecedented phases. At lower temperature, deeper in the symmetry-broken phase, higher-order terms in GL expansion of the free-energy become important. In this circumstance, the SDW/SBO configuration may cease to be uniaxial, promoting an octahedral spin configuration, which permits a more intriguing coupling of the order parameter to subleading magnetic fluctuations via the spin chirality coupling (cf. the SM). For charge-ordered phases, the coupling of real and imaginary bond order is known to promote subsidiary loop current orders [41,51]; here we draw an interesting parallel to magnetic instabilities. Spin currents are even under time-reversal symmetry (TRS). Hence, a coupling to SBO/SDW order can already appear at first-order in the spin-current order (SCO) parameter via the cubic term

$$\mathcal{F}^{(3)} \propto \sum_{\alpha\beta\gamma} \varepsilon_{\alpha\beta\gamma}\, \vec{\Delta}_{\alpha}^{s} \cdot \left(\vec{\Delta}_{\beta}^{s} \times \vec{\Delta}_{\gamma}^{\mathrm{SCO}}\right), \tag{5}$$

where $s = \{\mathrm{SBO},\mathrm{SDW}\}$. Minimizing this contribution to the free energy produces a state in which $\vec{\Delta}_{\alpha}^{s} \perp \vec{\Delta}_{\beta}^{s} \perp \vec{\Delta}_{\gamma}^{\mathrm{SCO}}$, i.e., the $\vec{\Delta}^{s}$ vectors at the three M points are mutually perpendicular, and locked parallel to the SCO vector, $\vec{\Delta}_{\alpha}^{s} \parallel \vec{\Delta}_{\alpha}^{\mathrm{SCO}}$. This locking between spin and M-point is a kind of "spontaneous spin-orbit coupling". Equation (5) is linear in $\vec{\Delta}^{\mathrm{SCO}}$, which implies that noncollinear $\vec{\Delta}^{s}$ is expected to immediately induce SCO, and conversely, the presence of SCO can induce canting of the $\vec{\Delta}^{s}$ state.

This mechanism for the emergence of spin current appears as a direct consequence of cascading phase transitions characteristic of kagome materials [52]. The only instance of spin currents reported to date is in FeGe, in the A-type AFM phase [53–55]. However, in that system the SCO can be simply viewed as loop current formation of spin-polarized electrons [14,56,57]. The new mechanism we describe above gives way to an uncharted territory of magnetic states due to the unique features of the kagome lattice, combining the effects of geometric frustration and SI in the moderately coupled regime.

VIII. SUMMARY

This study explores the emergence of itinerant magnetism in kagome lattice systems. Using $CsCu_3Cl_5$ as a theoretical platform, we achieve an electronic structure displaying the three characteristic kagome bands around the Fermi level almost without any interference from additional bands. A description by means of local reference frames enables the identification of a minimal tight-binding model using three maximally localized Wannier orbitals. While many kagome materials exhibit a more complex description, with several vHS near the Fermi level which may interplay to form novel electronic orders [10,11,45,58–60], our exemplary Cu-based kagome material $CsCu_3Cl_5$ exhibits an isolated m-type vHS close to the Fermi level, providing a model realization of the kagome Hubbard model that is worth exploring in future materials science experiments.

Our FRG study reveals an unprecedented unconventional $2 \times 2 \times 1$ antiferromagnetic ordering. While kagome magnets have attracted much attention in recent years, the formation of long-range magnetization is usually fostered by dipole interactions of localized magnetic moments rather than an intrinsic electronic mechanism such as that on display here [16,61]. In the presented scenario, quantum fluctuations provide the driving force for the magnetic transition. This expands the catalog of magnetic states on the kagome lattice: We predict a spin bond order phase with descendent spin current patterns on the kagome lattice, featuring a finite relative angular momentum of the spin-1 particle-hole pair in analogy to spin-0 charge bond order patterns. Our analysis marks the first chapter of emergent magnetic order from itinerant electrons on the kagome lattice, and it sets magnetic instabilities on the landscape of symmetry-broken phases in metallic kagome compounds.

ACKNOWLEDGMENTS

We thank S. Enzner, L. M. Schoop, J. B. Profe, and L. Klebl for valuable discussions and feedback on this work. A.W., M.D., H.H., and R.T. are supported by the Deutsche Forschungsgemeinschaft (DFG, German Research Foundation) through Project-ID 258499086 - SFB 1170, through the Würzburg-Dresden Cluster of Excellence on Complexity and

Topology in Quantum Matter - ct.qmat Project-ID 390858490 - EXC 2147, and the research unit QUAST, FOR 5249-449872909 (Project 3). A.C. acknowledges support from PNRR MUR project PE0000023-NQSTI. M.D. is grateful for support from a Ph.D scholarship of the Studienstiftung des Deutschen Volkes. A.W., A.C., D.D.S., and R.T. acknowledge the Gauss Centre for Supercomputing e.V. [87] for funding this project by providing computing time on the GCS Supercomputer SuperMUC-NG at Leibniz Supercomputing Centre [88], where the DFT and Wannier-based calculations were performed. M.D., H.H., and R.T. are grateful for HPC resources provided by the Erlangen National High Performance Computing Center (NHR@FAU) of the Friedrich-Alexander-Universität Erlangen-Nürnberg (FAU), which were used for the FRG calculations. NHR funding is provided by federal and Bavarian state authorities. NHR@FAU hardware is partially funded by the DFG - 440719683.

R.T. initiated and supervised the project. R.T., A.W., A.C., and F.v.R. designed the model system. A.W., A.C., and D.D.S. conducted the first-principles calculations and the related Wannier-based analysis. H.H. and M.D. performed the FRG calculations. M.D. carried out the GL analysis with input from H.D.S. and J.I., A.W., M.D., and J.I. wrote the manuscript with input from all authors.

DATA AVAILABILITY

Some of the data that support the findings of this article are openly available [75]. The output files of the FRG calculations at the end of the flow are not publicly available upon publication because it is not technically feasible and/or the cost of preparing, depositing, and hosting the data would be prohibitive within the terms of this research project. The data are available from the authors upon reasonable request.

[1] Y.-X. Jiang, J.-X. Yin, M. M. Denner, N. Shumiya, B. R. Ortiz, G. Xu, Z. Guguchia, J. He, M. S. Hossain, X. Liu, J. Ruff, L. Kautzsch, S. S. Zhang, G. Chang, I. Belopolski, Q. Zhang, T. A. Cochran, D. Multer, M. Litskevich, Z.-J. Cheng *et al.*, Unconventional chiral charge order in kagome superconductor KV_3Sb_5, Nat. Mater. **20**, 1353 (2021).

[2] C. Mielke, D. Das, J.-X. Yin, H. Liu, R. Gupta, Y.-X. Jiang, M. Medarde, X. Wu, H. C. Lei, J. Chang, P. Dai, Q. Si, H. Miao, R. Thomale, T. Neupert, Y. Shi, R. Khasanov, M. Z. Hasan, H. Luetkens, and Z. Guguchia, Time-reversal symmetry-breaking charge order in a kagome superconductor, Nature (London) **602**, 245 (2022).

[3] H. Li, S. Cheng, B. R. Ortiz, H. Tan, D. Werhahn, K. Zeng, D. Johrendt, B. Yan, Z. Wang, S. D. Wilson *et al.*, Electronic nematicity without charge density waves in titanium-based kagome metal, Nat. Phys. **19**, 1591 (2023).

[4] Z. Jiang, Z. Liu, H. Ma, W. Xia, Z. Liu, J. Liu, S. Cho, Y. Yang, J. Ding, J. Liu *et al.*, Flat bands, non-trivial band topology and rotation symmetry breaking in layered kagome-lattice $RbTi_3Bi_5$, Nat. Commun. **14**, 4892 (2023).

[5] P. K. Nag, R. Batabyal, J. Ingham, N. Morali, H. Tan, J. Koo, A. Consiglio, E. Liu, N. Avraham, R. Queiroz *et al.*, Pomeranchuk instability induced by an emergent higher-order Van Hove singularity on the distorted kagome surface of $Co_3Sn_2S_2$, arXiv:2410.01994.

[6] Y.-X. Jiang, S. Shao, W. Xia, M. M. Denner, J. Ingham, M. S. Hossain, Q. Qiu, X. Zheng, H. Chen, Z.-J. Cheng *et al.*, Van Hove annihilation and nematic instability on a kagome lattice, Nat. Mater. **23**, 1214 (2024).

[7] Y. Zhong, S. Li, H. Liu, Y. Dong, K. Aido, Y. Arai, H. Li, W. Zhang, Y. Shi, Z. Wang, S. Shin, H. N. Lee, H. Miao, T. Kondo, and K. Okazaki, Testing electron–phonon coupling for the superconductivity in kagome metal CsV_3Sb_5, Nat. Commun. **14**, 1945 (2023).

[8] Y. Xie, Y. Li, P. Bourges, A. Ivanov, Z. Ye, J.-X. Yin, M. Z. Hasan, A. Luo, Y. Yao, Z. Wang, G. Xu, and P. Dai, Electron-phonon coupling in the charge density wave state of CsV_3Sb_5, Phys. Rev. B **105**, L140501 (2022).

[9] M. L. Kiesel and R. Thomale, Sublattice interference in the kagome Hubbard model, Phys. Rev. B **86**, 121105(R) (2012).

[10] Y. Hu, X. Wu, B. R. Ortiz, S. Ju, X. Han, J. Ma, N. C. Plumb, M. Radovic, R. Thomale, S. D. Wilson, A. P. Schnyder, and M. Shi, Rich nature of Van Hove singularities in kagome superconductor CsV_3Sb_5, Nat. Commun. **13**, 2220 (2022).

[11] M. Kang, S. Fang, J.-K. Kim, B. R. Ortiz, S. H. Ryu, J. Kim, J. Yoo, G. Sangiovanni, D. Di Sante, B.-G. Park, C. Jozwiak, A. Bostwick, E. Rotenberg, E. Kaxiras, S. D. Wilson, J.-H. Park, and R. Comin, Twofold Van Hove singularity and origin of charge order in topological kagome superconductor CsV_3Sb_5, Nat. Phys. **18**, 301 (2022).

[12] M. L. Kiesel, C. Platt, and R. Thomale, Unconventional Fermi surface instabilities in the kagome Hubbard model, Phys. Rev. Lett. **110**, 126405 (2013).

[13] W.-S. Wang, Z.-Z. Li, Y.-Y. Xiang, and Q.-H. Wang, Competing electronic orders on kagome lattices at Van Hove filling, Phys. Rev. B **87**, 115135 (2013).

[14] J. Zhan, H. Hohmann, M. Dürrnagel, R. Fu, S. Zhou, Z. Wang, R. Thomale, X. Wu, and J. Hu, Loop current order on the kagome lattice, arXiv:2506.01648.

[15] F. Bert, A. Olariu, A. Zorko, P. Mendels, J. C. Trombe, F. Duc, M. A. de Vries, A. Harrison, A. D. Hillier, J. Lord, A. Amato, and C. Baines, Frustrated magnetism in the quantum kagome Herbertsmithite $ZnCu_3(OH)_6Cl_2$ antiferromagnet, J. Phys.: Conf. Ser. **145**, 012004 (2009).

[16] M. R. Norman, *Colloquium*: Herbertsmithite and the search for the quantum spin liquid, Rev. Mod. Phys. **88**, 041002 (2016).

[17] J. A. McGinnety, Cesium Tetrachlorocuprate. Structure, crystal forces, and charge distribution, J. Am. Chem. Soc. **94**, 8406 (1972).

[18] A. W. Schlueter, R. A. Jacobson, and R. E. Rundle, A redetermination of the crystal structure of $CsCuCl_3$, Inorg. Chem. **5**, 277 (1966).

[19] S. Hull and P. Berastegui, Crystal structures and ionic conductivities of ternary derivatives of the silver and copper monohalides-II: Ordered phases within the $(AgX)_x$–$(MX)_{1-x}$ and $(CuX)_x$–$(MX)_{1-x}$ (M = K, Rb and Cs; X = Cl, Br and I) systems, J. Solid State Chem. **177**, 3156 (2004).

[20] R. D. Shannon, Revised effective ionic radii and systematic studies of interatomic distances in halides and chalcogenides, Found. Crystallogr. **32**, 751 (1976).

[21] M. Veidis, G. Schreiber, T. Gough, and G. J. Palenik, Jahn-Teller distortions in octahedral copper (II) complexes, J. Am. Chem. Soc. **91**, 1859 (1969).

[22] See Supplemental Material at http://link.aps.org/supplemental/10.1103/fszl-7g57 for (i) stability analysis of the lattice structure and results on favored twisted configuration, (ii) computational details of the dft, frg, and gl calculations, and (iii) a discussion on the three-dimensional character of the band structure, which also includes Refs. [62–86].

[23] D. Werhahn, B. R. Ortiz, A. K. Hay, S. D. Wilson, R. Seshadri, and D. Johrendt, The kagomé metals $RbTi_3Bi_5$ and $CsTi_3Bi_5$, Z. Naturforsch. B **77**, 757 (2022).

[24] J. Yang, X. Yi, Z. Zhao, Y. Xie, T. Miao, H. Luo, H. Chen, B. Liang, W. Zhu, Y. Ye, J.-Y. You, B. Gu, S. Zhang, F. Zhang, F. Yang, Z. Wang, Q. Peng, H. Mao, G. Liu, Z. Xu *et al.*, Observation of flat band, Dirac nodal lines and topological surface states in kagome superconductor $CsTi_3Bi_5$, Nat. Commun. **14**, 4089 (2023).

[25] C. Bigi, M. Dürrnagel, L. Klebl, A. Consiglio, G. Pokharel, F. Bertran, P. L. Févre, T. Jaouen, H. C. Tchouekem, P. Turban, A. De Vita, J. A. Miwa, J. W. Wells, D. Oh, R. Comin, R. Thomale, I. Zeljkovic, B. R. Ortiz, S. D. Wilson, G. Sangiovanni *et al.*, Pomeranchuk instability from electronic correlations in $CsTi_3Bi_5$ kagome metal, arXiv:2410.22929.

[26] B. R. Ortiz, S. M. L. Teicher, L. Kautzsch, P. M. Sarte, N. Ratcliff, J. Harter, J. P. C. Ruff, R. Seshadri, and S. D. Wilson, Fermi surface mapping and the nature of charge-density-wave order in the kagome superconductor CsV_3Sb_5, Phys. Rev. X **11**, 041030 (2021).

[27] G. He, L. Peis, E. F. Cuddy, Z. Zhao, D. Li, Y. Zhang, R. Stumberger, B. Moritz, H. Yang, H. Gao, T. P. Devereaux, and R. Hackl, Anharmonic strong-coupling effects at the origin of the charge density wave in CsV_3Sb_5, Nat. Commun. **15**, 1895 (2024).

[28] F. Aryasetiawan, M. Imada, A. Georges, G. Kotliar, S. Biermann, and A. I. Lichtenstein, Frequency-dependent local interactions and low-energy effective models from electronic structure calculations, Phys. Rev. B **70**, 195104 (2004).

[29] T. Miyake, F. Aryasetiawan, and M. Imada, *Ab initio* procedure for constructing effective models of correlated materials with entangled band structure, Phys. Rev. B **80**, 155134 (2009).

[30] L. Vaugier, H. Jiang, and S. Biermann, Hubbard u and hund exchange j in transition metal oxides: Screening versus localization trends from constrained random phase approximation, Phys. Rev. B **86**, 165105 (2012).

[31] D. Di Sante, B. Kim, W. Hanke, T. Wehling, C. Franchini, R. Thomale, and G. Sangiovanni, Electronic correlations and universal long-range scaling in kagome metals, Phys. Rev. Res. **5**, L012008 (2023).

[32] I. I. Mazin, H. O. Jeschke, F. Lechermann, H. Lee, M. Fink, R. Thomale, and R. Valentí, Theoretical prediction of a strongly correlated Dirac metal, Nat. Commun. **5**, 4261 (2014).

[33] M. Jovanovic and L. M. Schoop, Simple chemical rules for predicting band structures of kagome materials, J. Am. Chem. Soc. **144**, 10978 (2022).

[34] B. R. Ortiz, S. M. L. Teicher, Y. Hu, J. L. Zuo, P. M. Sarte, E. C. Schueller, A. M. M. Abeykoon, M. J. Krogstad, S. Rosenkranz, R. Osborn, R. Seshadri, L. Balents, J. He, and S. D. Wilson, CsV_3Sb_5: A $\mathbb{Z}_2$ topological kagome metal with a superconducting ground state, Phys. Rev. Lett. **125**, 247002 (2020).

[35] Y. Liu, Z.-Y. Liu, J.-K. Bao, P.-T. Yang, L.-W. Ji, S.-Q. Wu, Q.-X. Shen, J. Luo, J. Yang, J.-Y. Liu, C.-C. Xu, W.-Z. Yang, W.-L. Chai, J.-Y. Lu, C.-C. Liu, B.-S. Wang, H. Jiang, Q. Tao, Z. Ren, X.-F. Xu *et al.*, Superconductivity under pressure in a chromium-based kagome metal, Nature (London) **632**, 1032 (2024).

[36] G. Sangiovanni, Superconductor surprises with strongly interacting electrons, Nature (London) **632**, 988 (2024).

[37] Y. Li, Y. Liu, X. Du, S. Wu, W. Zhao, K. Zhai, Y. Hu, S. Zhang, H. Chen, J. Liu, Y. Yang, C. Peng, M. Hashimoto, D. Lu, Z. Liu, Y. Wang, Y. Chen, G. Cao, and L. Yang, Electron correlation and incipient flat bands in the kagome superconductor $CsCr_3Sb_5$, Nat. Commun. **16**, 3229 (2025).

[38] S. Wu, C. Xu, X. Wang, H.-Q. Lin, C. Cao, and G.-H. Cao, Flat-band enhanced antiferromagnetic fluctuations and superconductivity in pressurized $CsCr_3Sb_5$, Nat. Commun. **16**, 1375 (2025).

[39] F. Xie, Y. Fang, Y. Li, Y. Huang, L. Chen, C. Setty, S. Sur, B. Yakobson, R. Valentí, and Q. Si, Electron correlations in the kagome flat band metal $CsCr_3Sb_5$, Phys. Rev. Res. **7**, L022061 (2025).

[40] Y. Wang, Heavy Fermions in frustrated Hund's metal with portions of incipient flat bands, Phys. Rev. B **111**, 035127 (2025).

[41] M. M. Denner, R. Thomale, and T. Neupert, Analysis of charge order in the kagome metal AV_3Sb_5 (A = K, Rb, Cs), Phys. Rev. Lett. **127**, 217601 (2021).

[42] J. B. Profe, L. Klebl, F. Grandi, H. Hohmann, M. Dürrnagel, T. Schwemmer, R. Thomale, and D. M. Kennes, The kagome Hubbard model from a functional renormalization group perspective, Phys. Rev. Res. **6**, 043078 (2024).

[43] Y. Wang, H. Wu, G. T. McCandless, J. Y. Chan, and M. N. Ali, Quantum states and intertwining phases in kagome materials, Nat. Rev. Phys. **5**, 635 (2023).

[44] S. Enzner, J. Berges, A. Schobert, D. Oh, M. Kang, R. Comin, R. Thomale, T. O. Wehling, D. Di Sante, and G. Sangiovanni, Phonon fluctuation diagnostics: Origin of charge order in Av_3Sb_5 kagome metals, arXiv:2504.07883.

[45] X. Wu, T. Schwemmer, T. Müller, A. Consiglio, G. Sangiovanni, D. Di Sante, Y. Iqbal, W. Hanke, A. P. Schnyder, M. M. Denner *et al.*, Phys. Rev. Lett. **127**, 177001 (2021).

[46] Q.-G. Yang, M. Yao, D. Wang, and Q.-H. Wang, Charge bond order and s-wave superconductivity in the kagome lattice with electron-phonon coupling and electron-electron interaction, Phys. Rev. B **109**, 075130 (2024).

[47] J. B. Profe, D. M. Kennes, and L. Klebl, divERGe implements various exact renormalization group examples, SciPost Phys. Codebases 26 (2024).

[48] W. Metzner, M. Salmhofer, C. Honerkamp, V. Meden, and K. Schönhammer, Functional renormalization group approach to correlated Fermion systems, Rev. Mod. Phys. **84**, 299 (2012).

[49] C. Platt, W. Hanke, and R. Thomale, Functional renormalization group for multi-orbital Fermi surface instabilities, Adv. Phys. **62**, 453 (2013).

[50] J. W. F. Venderbos, Symmetry analysis of translational symmetry broken density waves: Application to hexagonal lattices in two dimensions, Phys. Rev. B **93**, 115107 (2016).

[51] C. Guo, G. Wagner, C. Putzke, D. Chen, K. Wang, L. Zhang, M. Gutierrez-Amigo, I. Errea, M. G. Vergniory, C. Felser, M. H. Fischer, T. Neupert, and P. J. W. Moll, Correlated order at the tipping point in the kagome metal CsV_3Sb_5, Nat. Phys. **20**, 579 (2024).

[52] H. Zhao, H. Li, B. R. Ortiz, S. M. L. Teicher, T. Park, M. Ye, Z. Wang, L. Balents, S. D. Wilson, and I. Zeljkovic, Cascade of correlated electron states in the kagome superconductor CsV_3Sb_5, Nature (London) **599**, 216 (2021).

[53] J.-X. Yin, Y.-X. Jiang, X. Teng, M. S. Hossain, S. Mardanya, T.-R. Chang, Z. Ye, G. Xu, M. M. Denner, T. Neupert, B. Lienhard, H.-B. Deng, C. Setty, Q. Si, G. Chang, Z. Guguchia, B. Gao, N. Shumiya, Q. Zhang, T. A. Cochran *et al.*, Discovery of charge order and corresponding edge state in kagome magnet FeGe, Phys. Rev. Lett. **129**, 166401 (2022).

[54] X. Teng, L. Chen, F. Ye, E. Rosenberg, Z. Liu, J.-X. Yin, Y.-X. Jiang, J. S. Oh, M. Z. Hasan, K. J. Neubauer, B. Gao, Y. Xie, M. Hashimoto, D. Lu, C. Jozwiak, A. Bostwick, E. Rotenberg, R. J. Birgeneau, J.-H. Chu, M. Yi *et al.*, Discovery of charge density wave in a kagome lattice antiferromagnet, Nature (London) **609**, 490 (2022).

[55] X. Teng, J. S. Oh, H. Tan, L. Chen, J. Huang, B. Gao, J.-X. Yin, J.-H. Chu, M. Hashimoto, D. Lu, C. Jozwiak, A. Bostwick, E. Rotenberg, G. E. Granroth, B. Yan, R. J. Birgeneau, P. Dai, and M. Yi, Magnetism and charge density wave order in kagome FeGe, Nat. Phys. **19**, 814 (2023).

[56] S. Han, L. Li, C. S. Tang, Q. Wang, L. Zhang, C. Diao, M. Zhao, S. Sun, L. Tian, M. B. H. Breese, C. Cai, M. V. Milosevic, Y. Qi, A. T. S. Wee, and X. Yin, Orbital origin of magnetic moment enhancement induced by charge density wave in kagome FeGe, Appl. Phys. Rev. **12**, 031401 (2025).

[57] X. Teng, D. W. Tam, L. Chen, H. Tan, Y. Xie, B. Gao, G. E. Granroth, A. Ivanov, P. Bourges, B. Yan, M. Yi, and P. Dai, Spin-charge-lattice coupling across the charge density wave transition in a kagome lattice antiferromagnet, Phys. Rev. Lett. **133**, 046502 (2024).

[58] H. Li, Y. B. Kim, and H.-Y. Kee, Intertwined Van Hove singularities as a mechanism for loop current order in kagome metals, Phys. Rev. Lett. **132**, 146501 (2024).

[59] H. D. Scammell, J. Ingham, T. Li, and O. P. Sushkov, Chiral excitonic order from twofold Van Hove singularities in kagome metals, Nat. Commun. **14**, 605 (2023).

[60] J. Ingham, A. Consiglio, D. di Sante, R. Thomale, and H. D. Scammell, Theory of excitonic order in ScV_6Sn_6, arXiv:2410.16365.

[61] J.-X. Yin, B. Lian, and M. Z. Hasan, Topological kagome magnets and superconductors, Nature (London) **612**, 647 (2022).

[62] M. J. Winter, Webelements: The periodic table on the www (2023), https://winter.group.shef.ac.uk/webelements/chlorine/electronegativity.html.

[63] S. V. Streltsov and D. I. Khomskii, Orbital physics in transition metal compounds: New trends, Phys. Usp. **60**, 1121 (2017).

[64] A. Consiglio, T. Schwemmer, X. Wu, W. Hanke, T. Neupert, R. Thomale, G. Sangiovanni, and D. Di Sante, Van Hove tuning of AV_3Sb_5 kagome metals under pressure and strain, Phys. Rev. B **105**, 165146 (2022).

[65] H. LaBollita and A. S. Botana, Tuning the Van Hove singularities in $AV_3Sb_5(A = \mathrm{K}, \mathrm{Rb}, \mathrm{Cs})$ via pressure and doping, Phys. Rev. B **104**, 205129 (2021).

[66] C. Lin, A. Consiglio, O. K. Forslund, J. Kuspert, M. M. Denner, H. Lei, A. Louat, M. D. Watson, T. K. Kim, C. Cacho, D. Carbone, M. Leandersson, C. Polley, T. Balasubramanian, D. Di Sante, R. Thomale, Z. Guguchia, G. Sangiovanni, T. Neupert, and J. Chang, Giant strain response of charge modulation and singularity in a kagome superconductor, Nat. Commun. **15**, 10466 (2024).

[67] M. Tuniz, A. Consiglio, G. Pokharel, F. Parmigiani, T. Neupert, R. Thomale, G. Sangiovanni, S. D. Wilson, I. Vobornik, F. Salvador, F. Cilento, D. Di Sante, and F. Mazzola, Strain-induced enhancement of the charge-density-wave in the kagome metal ScV_6Sn_6, Phys. Rev. Lett. **134**, 066501 (2025).

[68] L. Ranalli, C. Verdi, L. Monacelli, G. Kresse, M. Calandra, and C. Franchini, Temperature-dependent anharmonic phonons in quantum paraelectric $KTaO_3$ by first principles and machine-learned force fields, Adv. Quantum Technol. **6**, 2200131 (2023).

[69] G. Kresse and D. Joubert, From ultrasoft pseudopotentials to the projector augmented-wave method, Phys. Rev. B **59**, 1758 (1999).

[70] G. Kresse and J. Furthmüller, Efficient iterative schemes for *ab initio* total-energy calculations using a plane-wave basis set, Phys. Rev. B **54**, 11169 (1996).

[71] J. P. Perdew, K. Burke, and M. Ernzerhof, Generalized gradient approximation made simple, Phys. Rev. Lett. **77**, 3865 (1996).

[72] V. Wang, N. Xu, J.-C. Liu, G. Tang, and W.-T. Geng, VASPKIT: A user-friendly interface facilitating high-throughput computing and analysis using VASP code, Comput. Phys. Commun. **267**, 108033 (2021).

[73] K. Momma and F. Izumi, VESTA: A three-dimensional visualization system for electronic and structural analysis, J. Appl. Crystallogr. **41**, 653 (2008).

[74] A. A. Mostofi, J. R. Yates, Y.-S. Lee, I. Souza, D. Vanderbilt, and N. Marzari, Wannier90: A tool for obtaining maximally-localised wannier functions, Comput. Phys. Commun. **178**, 685 (2008).

[75] Calculation data for first principle calculations are accessible at A. Wenger, A. Consiglio, H. Hohmann, M. Dürrnagel, F. O. von Rohr, H. D. Scammell, J. Ingham, Di Sante, and R. Thomale, Theory of unconventional magnetism in a Cu-based kagome metal [Data set], Zenodo (2025), https://doi.org/10.5281/zenodo.17483258.

[76] M. Kaltak, Merging GW with DMFT, Ph.D. thesis, Universität Wien, 2015.

[77] C. Honerkamp, Effective interactions in multiband systems from constrained summations, Phys. Rev. B **85**, 195129 (2012).

[78] J. B. Profe, J. Vučičević, P. P. Stavropoulos, M. Rösner, R. Valentí, and L. Klebl, Exact downfolding and its perturbative approximation, arXiv:2507.16916.

[79] M. Kaltak, A. Hampel, M. Schlipf, I. R. Reddy, B. Kim, and G. Kresse, Constrained random phase approximation: The spectral method, arXiv:2508.15368.

[80] J. Lichtenstein, D. Sánchez de la Peña, D. Rohe, E. Di Napoli, C. Honerkamp, and S. A. Maier, High-performance functional renormalization group calculations for interacting Fermions, Comput. Phys. Commun. **213**, 100 (2017).

[81] J. Beyer, J. B. Profe, and L. Klebl, Reference results for the momentum space functional renormalization group, Eur. Phys. J. B **95**, 65 (2022).

[82] J. B. Profe and D. M. Kennes, TU^{2}FRG: A scalable approach for truncated unity functional renormalization group in generic Fermionic models, Eur. Phys. J. B **95**, 60 (2022).

[83] T. Park, M. Ye, and L. Balents, Electronic instabilities of kagome metals: Saddle points and Landau theory, Phys. Rev. B **104**, 035142 (2021).

[84] R. Nandkishore, G.-W. Chern, and A. V. Chubukov, Itinerant half-metal spin-density-wave state on the hexagonal lattice, Phys. Rev. Lett. **108**, 227204 (2012).

[85] C. Xu, S. Wu, G.-X. Zhi, G. Cao, J. Dai, C. Cao, X. Wang, and H.-Q. Lin, Frustrated altermagnetism and charge density wave in kagome superconductor $CsCr_3Sb_5$, Nat. Commun. **16**, 3114 (2025).

[86] L. Messio, C. Lhuillier, and G. Misguich, Lattice symmetries and regular magnetic orders in classical frustrated antiferromagnets, Phys. Rev. B **83**, 184401 (2011).

[87] https://www.gauss-centre.eu.

[88] https://www.lrz.de.